

# The free surface of superfluid $^4\text{He}$ at zero temperature

J. M. Marín, J. Boronat, and J. Casulleras

*Departament de Física i Enginyeria Nuclear, Universitat Politècnica  
de Catalunya, Campus Nord B4-B5, E-08034 Barcelona, Spain*

(Dated: June 22, 2018)

The structure and energetics of the free surface of superfluid  $^4\text{He}$  are studied using the diffusion Monte Carlo method. Extending a previous calculation by Vallés and Schmidt, which used the Green's function Monte Carlo method, we study the surface of liquid  $^4\text{He}$  within a slab geometry using a larger number of particles in the slab and an updated interatomic potential. The surface tension is accurately estimated from the energy of slabs of increasing surface density and its value is close to one of the two existing experimental values. Results for the density profiles allow for the calculation of the surface width which shows an overall agreement with recent experimental data. The dependence on the transverse direction to the surface of other properties such as the two-body radial distribution function, structure factor, and one-body density matrix is also studied. The condensate fraction, extracted from the asymptotic behavior of the one-body density matrix, shows an unambiguous enhancement when approaching the surface.

PACS numbers: 67.40.Rp, 68.03.Cd, 02.70.Ss

## I. INTRODUCTION

The interest of quantum many-body theory in inhomogeneous superfluid  $^4\text{He}$  has been active for many years and continuously enriched by the achievement of new experimental realizations of confining geometries.<sup>1</sup> The most classical, and consequently best known, correspond to  $^4\text{He}$  films adsorbed on different substrates<sup>2,3</sup> and to  $^4\text{He}$  clusters produced by free jet expansions through very thin nozzles.<sup>4</sup> More recently, and still with some open questions, interest has been devoted to  $^4\text{He}$  in porous media such as vycor or aerogel<sup>5,6,7</sup> and  $^4\text{He}$  adsorbed in carbon nanotube bundles<sup>8,9,10,11,12</sup> forming quasi-one-dimensional structures. In common with other fluids currently under study, the effects of a confined geometry upon its microscopic properties are most interesting. Additionally, liquid  $^4\text{He}$  poses an unavoidable quantum behavior which manifests in its own existence as a liquid even at zero temperature, with a superfluid phase and a partially occupied Bose-Einstein state. Moreover, its extreme purity allows for a much cleaner extraction of data which is usually impossible with other liquids.

One of the fundamental features raised by the inhomogeneous situations described above is the emergence of the free surface of superfluid  $^4\text{He}$ .<sup>13</sup> For a long time, the main concern has been to understand how distinctive properties of this quantum liquid, like its superfluid density and condensate fraction, behave when the density goes to zero through a free surface.<sup>14</sup> Also the surface tension, the form of its density profile, the value of the surface width, and the role of the surface excitations in its dynamics have been theoretically and experimentally studied.<sup>3,15,16,17,18</sup> The most direct information on the density profile and interfacial width has been obtained by x-ray reflectivity<sup>19,20,21</sup> and ellipsometric<sup>22</sup> measurements. The latter was carried out by Osborne,<sup>22</sup> who assuming a Fermi function for the profile, extracted a 10-90 % width of 9.4 Å at 1.8 K. The most recent data

correspond to the x-ray measurement of Penanen *et al.*<sup>21</sup> who reported a value 6.5 Å at 0.45 K, a lower temperature than the first measure performed by Lurio *et al.*<sup>20</sup> at 1.13 K who reported a wider surface of 9.1 Å. The relative spread of the experimental results on the microscopic characteristics of the density profile points out the difficulties which experimental setups face to carry out a clean extraction of the data and its reduction to the ground state, i.e., to zero temperature.

The difficulty of the experimental work on the study of the  $^4\text{He}$  free surface is also reflected in the long-time effort to measure accurately the surface tension. Since the first work by Urk *et al.*<sup>23</sup> in 1925, the number of groups and different techniques used for this measure is unusually large. Recent data starts with Iino *et al.*<sup>24</sup> who measured the surface tension using the surface-wave resonance method obtaining an estimation at zero temperature of  $\sigma = 0.257 \text{ K}\text{Å}^{-2}$ . Later on, Roche *et al.*<sup>25</sup> obtained a slightly larger value  $\sigma = 0.274 \text{ K}\text{Å}^{-2}$  from the frequencies of capillary waves with wavelength in the micron range. In this second work, the difference in the values obtained for  $\sigma$  is imputed to a possible inaccuracy in the work of Iino *et al.*<sup>24</sup> related to the treatment of the meniscus at the edge of the box. However, this argument was refuted posteriorly by Nakanishi and Suzuki<sup>26</sup> who confirmed the result obtained in Ref. 24. Recently, Vicente *et al.*<sup>27</sup> performed a new measure of the surface tension using the vibration modes of levitated  $^4\text{He}$  drops, and the result was in perfect agreement with the larger value obtained by Roche *et al.*<sup>25</sup>

The surface tension, surface width, and density profile of the free  $^4\text{He}$  surface have been calculated using both density functional<sup>16,28,29</sup> and microscopic theory.<sup>15,30,31,32,33</sup> Density functional theory relies on functional forms of the energy which depend on the one-body density and some parameters which are adjusted to reproduce selected experimental data. These functionals have been progressively improved by the inclusion of non-local

contributions and specific terms to reproduce the experimental static response function.<sup>16</sup> Contrarily to the first models, in which the surface tension was considered an input to fix parameters, the most modern ones are able to give predictions for  $\sigma$ . The results for the surface tension are in an overall agreement with the experimental data from Ref. 25, and the surface width is  $\sim 6$  Å. The methodology of microscopic approaches is different since the starting point in all of them is the Hamiltonian of the liquid containing realistic interparticle interactions. In this respect, the variational method has been specially useful due to the hard-core of the He-He interaction. In fact, the most extensive work in the field of inhomogeneous  $^4\text{He}$  has been carried out in the variational framework of the hypernetted chain (HNC) and correlated basis function (CBF) theories. Of special relevance in this field is the continued work by Krotscheck and co-workers,<sup>34</sup> who have carried out a nearly exhaustive study of  $^4\text{He}$  in reduced geometries both for the ground and the excited states.

Quantum Monte Carlo methods<sup>35</sup> have also been applied to the study of the free surface of liquid  $^4\text{He}$ . Using a slab geometry, Vallés and Schmidt<sup>32</sup> calculated the ground-state properties of the surface by means of the variational Monte Carlo (VMC) method with a trial wave function containing two- and three-body correlations. They extracted a surface tension  $\sigma = 0.272 \text{ KÅ}^{-2}$  (again very close to data from Ref. 25) from an analytical fit to the dependence of the energy with the inverse of the surface density. Galli and Reatto<sup>36</sup> studied a  $^4\text{He}$  slab using a shadow wavefunction and the VMC method; they obtained  $\sigma = 0.31(1) \text{ KÅ}^{-2}$  and a surface thickness  $\sim 5$  Å. The variational constraints can be removed by applying the essentially exact diffusion Monte Carlo (DMC) and Green's function Monte Carlo (GFMC) methods. At present, the only application of these methods to a slab corresponds to a GFMC calculation by Vallés and Schmidt<sup>32</sup> who estimated a surface tension of  $0.265 \text{ KÅ}^{-2}$  and a small value for the width ( $\sim 4$  Å) probably due to the small number of particles used in the simulation. Recently, Draeger and Ceperley<sup>33</sup> carried out a similar study but at finite temperature using the path integral Monte Carlo (PIMC) method. This work does not contain results for  $\sigma$  and surface width since its main motivation was the study of the enhancement of the Bose-Einstein condensate fraction at the surface.

In the last years, a renewed interest in the study of the  $^4\text{He}$  surface has emerged since the first theoretical observation by Lewart *et al.*<sup>37</sup> of a large increase of the condensed fraction near the surface of  $^4\text{He}$  drops. The relevance of this result in the long way for searching a Bose-Einstein condensed state was put forward by Griffin and Stringari<sup>38</sup> who studied the low density surface using a generalized Gross-Pitaevskii equation. A subsequent work by Galli and Reatto,<sup>36</sup> using the VMC method with a trial wave function based on the shadow model, pointed out that the introduction of fluctuations on the surface,

mainly the zero point motion of ripplons, can reduce significantly the enhancement of  $n_0$ . Their results show an increase of  $n_0$  up to a maximum value 0.5 and a decrease to zero when the density  $\rho(r)$  approaches zero. In order to shed light on these two different predictions, Draeger and Ceperley<sup>33</sup> calculated  $n_0$  in a  $^4\text{He}$  slab using PIMC. Their results show also a clear enhancement of the condensate fraction up to values larger than 0.9 and a small decrease when approaching the outer part of the surface. Therefore, fluctuations can arise and reduce  $n_0$  but their effects could be significantly smaller than in the VMC calculation of Ref. 36. A conclusive statement would require from a direct experimental measure which, for example, in the bulk has not yet been possible. Nevertheless, at present there are two experiments that seem to confirm the increase of  $n_0$ . The first one was derived from a quantum evaporation experiment,<sup>39</sup> and the second and more recent, from deep-inelastic neutron scattering on thick layers of  $^4\text{He}$  on an MgO substrate.<sup>40</sup>

In the present paper, we present a DMC calculation of the ground-state properties of a free  $^4\text{He}$  surface at zero temperature. To some extent, our work represents an update of the GFMC calculation of Vallés and Schmidt<sup>32</sup> in the sense of considering a more accurate interatomic potential and a larger number of particles in the simulation to achieve thicker slabs and therefore a more realistic study of the surface. Moreover, we have included in the present study topics like the density profile form, two-body distribution functions and structure factors, and mainly the study of the one-body density matrix which were not analyzed in Ref. 32. The exact character of the DMC method, within the statistical noise, allows for an accurate study of all the surface properties without the bounds imposed by a variational treatment. The methodology used in the analysis is, regarding the main inputs, the same that we have used previously in the study of bulk liquid  $^4\text{He}$  and  $^3\text{He}$ , and that has shown an overall agreement between theory and experiment.<sup>41</sup>

Our paper is organized as follows. In the next section, we review the DMC method which works with a second-order approximation for the short-time Green function. The specific details of the simulation for the slab geometry are also discussed, with special emphasis on the requirements for the trial wave function used for importance sampling. The results obtained, for both structure and energetics of the slab, are presented in Section III. Finally, Section IV comprises additional discussion on the results and the main conclusions.

## II. DIFFUSION MONTE CARLO AND THE SLAB GEOMETRY

The DMC method is nowadays a well established tool for solving the many-body imaginary-time Schrödinger equation,

$$-\frac{\partial \Psi(\mathbf{R}, t)}{\partial t} = (H - E) \Psi(\mathbf{R}, t), \quad (1)$$

where  $\mathbf{R} \equiv (\mathbf{r}_1, \dots, \mathbf{r}_N)$  is a  $3N$ -dimensional vector (*walker*) and  $t$  is the imaginary time measured in units of  $\hbar$ . The time-dependent wave function of the system  $\Psi(\mathbf{R}, t)$  can be expanded in terms of a complete set of eigenfunctions  $\phi_i(\mathbf{R})$  of the Hamiltonian,

$$\Psi(\mathbf{R}, t) = \sum_n c_n \exp[-(E_i - E)t] \phi_i(\mathbf{R}), \quad (2)$$

where  $E_i$  is the eigenvalue associated to  $\phi_i(\mathbf{R})$ . The asymptotic solution of Eq. (1), for any value  $E$  close to the energy of the ground state and for long times ( $t \rightarrow \infty$ ), gives  $\phi_0(\mathbf{R})$ , provided that there is a nonzero overlap between  $\Psi(\mathbf{R}, t=0)$  and the ground-state wave function  $\phi_0(\mathbf{R})$ .

An efficient solution of Eq. (1) requires from the use of importance sampling. It is introduced by solving the Schrödinger equation for the wave function

$$f(\mathbf{R}, t) \equiv \psi(\mathbf{R}) \Psi(\mathbf{R}, t), \quad (3)$$

$\psi(\mathbf{R})$  being a time-independent trial wave function able to describe the system at a variational level. Introducing the Hamiltonian of the system

$$H = -\frac{\hbar^2}{2m} \nabla_{\mathbf{R}}^2 + V(\mathbf{R}), \quad (4)$$

Eq. (1) turns out to be

$$-\frac{\partial f(\mathbf{R}, t)}{\partial t} = -D \nabla_{\mathbf{R}}^2 f(\mathbf{R}, t) + D \nabla_{\mathbf{R}}(\mathbf{F}(\mathbf{R}) f(\mathbf{R}, t)) + (E_L(\mathbf{R}) - E) f(\mathbf{R}, t), \quad (5)$$

with  $D = \hbar^2/(2m)$ ,  $E_L(\mathbf{R}) = \psi(\mathbf{R})^{-1} H \psi(\mathbf{R})$  the local energy, and

$$\mathbf{F}(\mathbf{R}) = 2\psi(\mathbf{R})^{-1} \nabla_{\mathbf{R}} \psi(\mathbf{R}) \quad (6)$$

is the drift force which guides the diffusion process.

The r.h.s. of Eq. (5) may be written as the action of three operators  $A_i$  acting on the wave function  $f(\mathbf{R}, t)$ ,

$$-\frac{\partial f(\mathbf{R}, t)}{\partial t} = (A_1 + A_2 + A_3) f(\mathbf{R}, t) \equiv A f(\mathbf{R}, t) \quad (7)$$

The first one,  $A_1$ , corresponds to a free diffusion with a diffusion coefficient  $D$ ;  $A_2$  acts as a driving force due to an external potential, and finally  $A_3$  looks like a birth/death term. Equation (7) is transformed to the integral form

$$f(\mathbf{R}', t + \Delta t) = \int G(\mathbf{R}', \mathbf{R}, \Delta t) f(\mathbf{R}, t) d\mathbf{R}, \quad (8)$$

by introducing the Green function

$$G(\mathbf{R}', \mathbf{R}, \Delta t) = \langle \mathbf{R}' | \exp(-A\Delta t) | \mathbf{R} \rangle. \quad (9)$$

with  $A \equiv A_1 + A_2 + A_3$ .

In the DMC method, Eq. (9) is iterated repeatedly until to reach the asymptotic regime  $f(\mathbf{R}, t \rightarrow \infty)$ , a limit

in which one is effectively sampling the ground state. In our implementation of the method we use a second-order expansion (quadratic DMC),<sup>42</sup>

$$\begin{aligned} \exp(-A\Delta t) = & \exp\left(-A_3 \frac{\Delta t}{2}\right) \exp\left(-A_2 \frac{\Delta t}{2}\right) \exp(-A_1 \Delta t) \\ & \times \exp\left(-A_2 \frac{\Delta t}{2}\right) \exp\left(-A_3 \frac{\Delta t}{2}\right) + \mathcal{O}((\Delta t)^3), \end{aligned} \quad (10)$$

which has proved to be a good compromise between algorithmic complexity and efficiency.

The study of the free surface is made by simulating a slab which grows symmetrically in the  $z$  direction and with periodic boundary conditions in the  $x$ - $y$  plane. The slab geometry is probably the best suited one to analyze the free surface since it does not present neither the substrate influence of films nor the curvature effects of drops. It is also true that the existence of two surfaces can introduce some residual influence between them. However, we have checked in our simulations that this effect, at least for the larger slabs, is completely negligible.

The implementation of DMC requires of a model for the trial wave function  $\psi(\mathbf{R})$  with the basic physical features of the system under study. In the present case, one *a priori* knows that  $\psi(\mathbf{R})$  becomes zero in two situations: when two atoms get closer than the core of its interaction, and when an atom tries to escape from the surface. Notice that at zero temperature no vapor is present out of the liquid. Having in mind these arguments, we consider

$$\psi(\mathbf{R}) = \psi_J(\mathbf{R}) \phi(\mathbf{R}), \quad (11)$$

with a Jastrow correlation factor accounting for dynamical correlations

$$\psi_J(\mathbf{R}) = \prod_{i < j}^N f(r_{ij}), \quad (12)$$

and a confining term, factorized in the form

$$\phi(\mathbf{R}) = \prod_{i=1}^N h(z_i). \quad (13)$$

The two-body correlation function is the same we used in the study of the bulk liquid.<sup>42</sup> It was proposed by Reatto<sup>43</sup> and incorporates, in an approximate way, the medium range behavior of  $f(r)$  observed in the Euler-Lagrange functional optimization,

$$f(r) = \exp\left[-\frac{1}{2} \left(\frac{b}{r}\right)^5 - \frac{L}{2} \exp\left[-\left(\frac{r-\lambda}{\Lambda}\right)^2\right]\right]. \quad (14)$$

The confining function is chosen of Fermi type, like in Refs. 32 and 44,

$$h(z) = \{1 + \exp[k(|z - z_{\text{cm}}| - z_0)]\}^{-1}, \quad (15)$$

with parameters  $k$  and  $z_0$  controlling the width and location of the interface, respectively. Possible and spurious kinetic energy contributions due to the movement of the center of mass are removed by subtracting  $z_{\text{cm}}$  to each particle coordinate  $z$  in Eq. (15).

### III. RESULTS

The properties of the free surface of liquid  $^4\text{He}$  have been studied by performing DMC calculations with an increasing number of particles  $N=54, 108, 162, 216, 324$ , and a fixed  $x-y$  area of  $A = 290.3 \text{ \AA}^2$ . The interatomic potential is the HFD-B(HE) model proposed by Aziz *et al.*<sup>45</sup> that has proven its high accuracy in previous DMC calculations of the density dependence of the pressure and speed of sound in bulk  $^4\text{He}$  and  $^3\text{He}$  liquids.<sup>41</sup> As a matter of comparison with the GFMC calculation of Vallés and Schmidt,<sup>32</sup> and in order to establish the influence of the potential in the surface properties, we have calculated the energy of the system and the surface tension using the HFDHE2 model, also proposed by Aziz and collaborators.<sup>46</sup>

In order to take into account size effects, due to the finite value of the simulation area  $A$  and periodic boundary conditions in the  $x-y$  plane, we have added to the energy tail corrections which are externally calculated assuming that the particles are uncorrelated for distances in this plane larger than half of the simulation square. The analytical expressions for the tails are reported in Ref. 32. Applying this analysis, we have verified that the energy per particle when doubling simultaneously  $A$  and  $N$  does not change within the current statistical noise. Possible bias in the DMC calculations coming from the time step and the mean population of walkers are also under control working, in both cases, with values which are well in the asymptotic regime.

A final key point of a DMC simulation concerns the values of the parameters in the trial wave function (14,15). This has been dealt by performing a series of VMC calculations and searching the optimal set. As expected, the only parameter which clearly shows a dependence on the number of particles, i.e., the size of the slab, is  $z_0$ ; the particular values are reported in Table I. The rest of the set has shown negligible dependence on  $N$ ; their values are  $b = 3.067 \text{ \AA}$ ,  $L = 0.2$ ,  $\lambda = 5.112 \text{ \AA}$ ,  $\Lambda = 1.534 \text{ \AA}$ , and  $k = 1 \text{ \AA}^{-1}$ .

#### A. Energies and surface tension

The DMC results of the energy per particle as a function of the number of particles included in the simulation, with a fixed area  $A$ , is reported in Table I. The coverage densities  $n_c$ , defined as

$$n_c = \frac{N}{A} = \int_{-\infty}^{\infty} dz \rho(z), \quad (16)$$

$N$	$n_c$ ( $\text{\AA}^{-2}$ )	$z_0$ ( $\text{\AA}$ )	$E/N$ (K)	$T/N$ (K)	$E^I/N$
54	0.1860	3.60	-4.519(6)	7.191(13)	-4.40
80	0.2756	5.41	-5.287(6)	8.562(15)	-5.15
108	0.3720	7.30	-5.763(8)	9.515(32)	-5.63
162	0.5580	10.95	-6.261(7)	10.950(34)	-6.12
216	0.7441	14.60	-6.528(6)	11.720(34)	-6.39
324	1.1161	22.10	-6.766(11)	13.075(40)	-6.63
	$\infty$		-7.267(13)	14.32(5)	-7.12

TABLE I: Total ( $E/N$ ) and kinetic ( $T/N$ ) energies per particle as a function of the number of particles  $N$  and the coverage density  $n_c$ .  $E^I/N$  is calculated with the old Aziz potential (HFDHE2);<sup>46</sup> the results in squared parenthesis are taken from Ref. 32. Figures in parenthesis are the statistical errors.  $z_0$  is a variational parameter present in the correlation factor  $h(z)$  (15). The bulk result is taken from Ref. 42

with  $\rho(z)$  the density profile, are also contained in the Table. When  $n_c$  increases, the energies approach the bulk value<sup>42</sup> which appears in the last row to help in the comparison. In the last column, we have included results for the energy using the old Aziz (HFDHE2) potential. As it is known from previous DMC calculations for the bulk,<sup>42</sup> the energies obtained with the HFDHE2 potential are slightly smaller (in absolute value), the difference with the HFD-B(HE) model being mainly due to the increase in the potential energy. Results for the kinetic energy, which are the same for the two potentials within error bars, are included in the Table showing convergence to the bulk value (14.32 K).<sup>47</sup> Enclosed in squared brackets in the Table there are GFMC results from Ref. 32 calculated at the same coverages; the agreement with our results is better for the larger coverage case but the lack of data at larger  $n_c$  leaves the comparison rather incomplete in the most interesting region, i.e., for the largest slabs.

The energies per particle, as a function of the inverse of the surface coverage ( $1/n_c$ ), are shown in Fig. 1. As a limiting case ( $n_c = \infty$ ), the energies corresponding to the bulk for the two potentials are also plotted. Under general assumptions it is expected that the energy per particle in the slab follows a polynomial expansion in terms of  $1/n_c$ ,<sup>29</sup>

$$\left(\frac{E}{N}\right) = \left(\frac{E}{N}\right)_{\infty} + \frac{2\sigma}{n_c} + \frac{\gamma}{n_c^3} + \mathcal{O}\left(\frac{1}{n_c^4}\right). \quad (17)$$

In this expansion,  $\sigma$  is the surface tension and the parameter  $\gamma$  has been related to the long-range interaction term of an hypothetical  $^4\text{He}$  substrate.<sup>29</sup> In Fig. 1 (top), the energies for slabs with different number of atoms are shown for values  $1/n_c < 3 \text{ \AA}^2$ . In this regime, corresponding to the largest slabs, the energy is a linear function of  $1/n_c$ . A linear fit to the data, for both interatomic potentials, gives  $\chi^2/\nu = 1 - 1.5$ . From the linear coefficient we estimate the surface tension; for the most accurate HFD-B(HE) potential  $\sigma = 0.281(3) \text{ K\AA}^{-2}$ , and  $\sigma = 0.278(3) \text{ K\AA}^{-2}$  for the old Aziz potential. Within

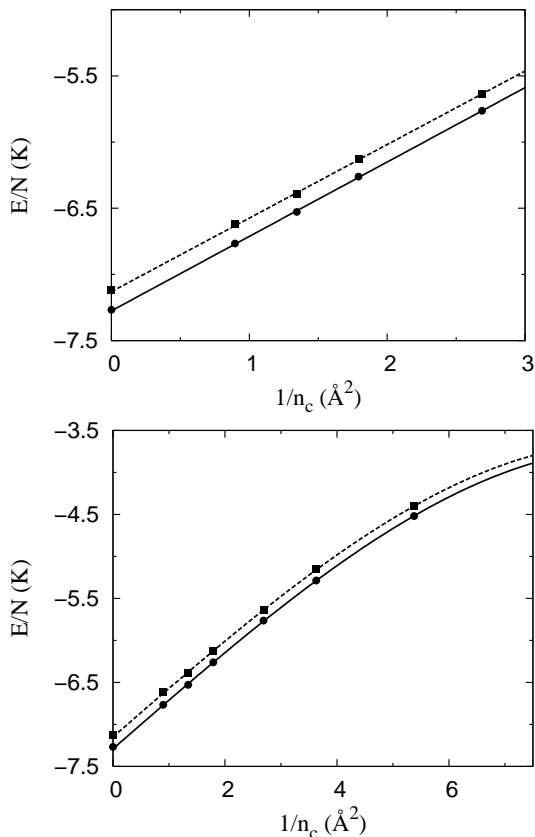


FIG. 1: Energies per particle as a function of the inverse of the surface coverage. Circles and squares stand for the calculations with the HFD-B(HE) and the HFDHE2 potentials, respectively. *Top*: Large  $n_c$  regime; solid and dashed lines correspond to numerical fits (17) with  $\gamma = 0$ . *Bottom*: All the coverages; the lines are numerical fits (17) to the DMC data with  $\gamma \neq 0$ .

the statistical errors, the surface tension is the same for both potentials implying that changing the potential introduces a shift in the energy which is to a large extent independent of the number of atoms. In the fit, the DMC energy of the bulk phase, corresponding to  $1/n_c = 0$ , has been included. However, it turns out that the inclusion or not of the bulk energy in the fit does not modify the result for the surface tension, and that the extrapolated energy to  $1/n_c = 0$  matches the bulk result, a feature that gives us additional confidence on the accuracy of the slab energies.

In order to describe the whole data set it is necessary to introduce in the fit higher-order terms (17). To this end, we have introduced a next-order term with  $1/n_c^2$  or  $1/n_c^3$ , and tried to discriminate which of the two options is more favored by our data. Using the third-power, as suggested by Szybisz<sup>29</sup> (17), the resulting value for  $\chi^2/\nu$  is 2.5, a value significantly smaller than the one achieved with a quadratic law (8.0). Therefore, and in spite of not being completely conclusive, our data support Szybisz's analysis. The corresponding fits are shown together with the DMC data in Fig. 1 (bottom). The surface tension

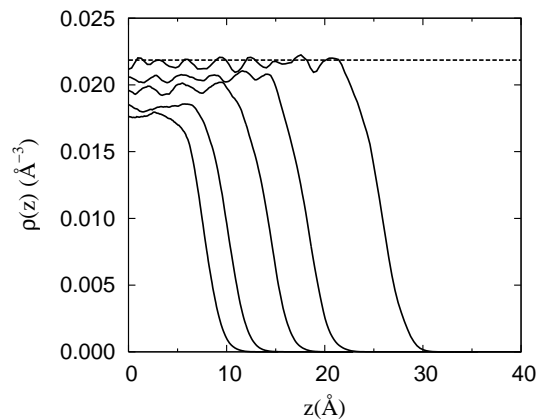


FIG. 2: Density profiles for an increasing number of particles in the slab. From left to right, they correspond to  $N = 80, 108, 162, 216,$  and  $324$  atoms. The dashed line shows the equilibrium density of the homogeneous liquid,  $\rho_0 = 0.02186 \text{ \AA}^{-3}$ .

from this fit is  $\sigma = 0.291(4) \text{ K\AA}^{-2}$ , nearly compatible with our best prediction from the linear fit to the largest  $n_c$  values. On the other hand,  $\gamma = -0.0023(2) \text{ K\AA}^{-6}$  roughly half the approximated value obtained by Szybisz.

The present result for the surface tension is a bit larger than the one obtained by Vallés and Schmidt in a GFMC calculation with the old Aziz potential (HFDHE2),  $\sigma = 0.265(6) \text{ K\AA}^{-2}$ .<sup>32</sup> That difference can be attributed to the fact that we have available data corresponding to large  $n_c$  values, which is crucial for the estimation of  $\sigma$ , and somehow also to the use they made of a second-order polynomial fit. Chin and Krotscheck<sup>30</sup> obtained  $\sigma = 0.284 \text{ K\AA}^{-2}$  in an Euler-Lagrange optimized HNC calculation of  $^4\text{He}$  clusters. Density functional theory including non-local terms are predictive for the surface tension;<sup>16</sup> the different functionals in the literature<sup>29</sup> show results for the surface tension in the range  $0.272\text{-}0.287 \text{ K\AA}^{-2}$ .

## B. Density profile

Results for the density profiles of the slab, with different number of atoms in the simulation cell, are shown in Fig. 2. In order to eliminate any residual bias, due to the importance sampling trial wave function, pure estimators have been used.<sup>47</sup> When  $N$  increases, the surface moves along  $z$  and the density in the central part increases progressively towards the equilibrium density of bulk  $^4\text{He}$  ( $\rho_0 = 0.02186 \text{ \AA}^{-3}$ ). This density is nearly reached for our largest slab corresponding to  $N = 324$  atoms. The oscillation in density which appears in the inner part of the slab does not have any physical meaning since its amplitude is compatible with the statistical noise there. The existence of stable oscillations in the surface has been discussed in several works after the first proposal by Regge.<sup>48</sup> Within the present accuracy,

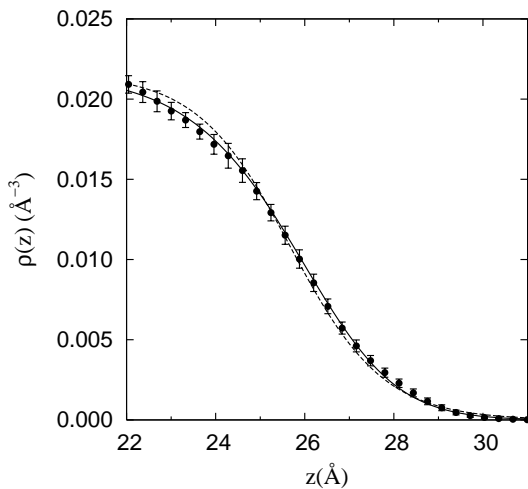


FIG. 3: Symetric vs. asymmetric fit to the  ${}^4\text{He}$  density profile. Points with errorbars are the computed values for the slab with  $N = 324$ . The dashed and solid lines correspond to a symmetric ( $\delta = 1$  in Eq. (18)) and an asymmetric model ( $\delta \neq 1$ ), respectively.

our results exclude this possibility. Nevertheless, the results contained in Fig. 2 show a slight shoulder in the inner part of the surface (hardly observable for the smallest slabs) that could resemble a Regge oscillation. This property of the  ${}^4\text{He}$  density profile has been observed previously in semi-infinite matter and clusters.<sup>16,30</sup>

The different slope of the density profile in the inner and outer parts of the surface has been observed and discussed in previous works. This feature is directly related to the possible asymmetry of  $\rho(z)$ .<sup>17,18,20</sup> In order to guide our analysis on this point, and trying to be quantitatively accurate, we have fitted to the DMC data functions of the type

$$\rho(z) = \frac{\rho_0}{(1 + e^{\beta(z-z_0)})^\delta}. \quad (18)$$

If  $\delta = 1$  in Eq. (18) the density profile is symmetric; otherwise, the model is asymmetric with a degree of asymmetry governed by  $\delta$ . Using  $\chi^2$  as a goodness parameter, we have observed that the DMC data for the larger slabs ( $N \geq 162$ ) is best reproduced by an asymmetric fit. On the contrary, for the smaller and less realistic slabs, the quality of the fit is not improved if  $\delta \neq 1$ . In Fig. 3, symmetric and asymmetric fits to the DMC data on the slab with  $N = 324$  are shown on top of the simulation results. The differences between the two fits are certainly small but the asymmetric model matches better the DMC results, especially in the inner part of the surface where the slope of the profile is less pronounced. An additional argument of consistency towards the assessment of an asymmetric profile is the stability in the value of  $\delta$  which is the same for the three larger slabs,  $\delta = 1.91(15)$ .

One of the most relevant properties characterizing the surface is its width, usually measured as the length ( $W$ ) over which the density decreases from 90 to 10 % of the

$N$	$\rho_0$ ( $\text{\AA}^{-3}$ )	$W$ ( $\text{\AA}$ )	$z_{1/2}$ ( $\text{\AA}$ )
80	0.0177(2)	3.66(5)	7.75(5)
108	0.0184(2)	4.01(5)	10.09(5)
162	0.0198(2)	4.57(5)	14.19(5)
216	0.0206(2)	4.76(5)	18.06(5)
324	0.0217(2)	5.07(5)	25.74(5)

TABLE II: Central density ( $\rho_0$ ), surface width ( $W$ ), and size of the slab measured with  $z_{1/2}$ , as a function of the number of atoms  $N$ .

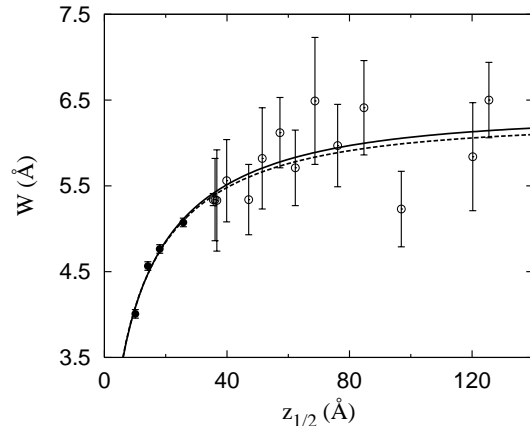


FIG. 4: Interfacial width  $W$  as a function of the size of the slab, measured in terms of  $z_{1/2}$  (solid circles). The open circles correspond to experimental data from Penanen *et al.*<sup>21</sup> The solid line is the fit (19) considering only our theoretical data and the dashed line corresponds to the same analytical form but including also the experimental points.

inner constant value. Theoretical calculations of the  ${}^4\text{He}$  free surface at zero temperature using microscopic theory<sup>15,30,31,32,33</sup> or density functional approaches<sup>16,28,29</sup> predict values in the range 5-7  $\text{\AA}$ . These results are in overall agreement with the most recent experimental data at  $T = 0.45$  K, which point to a width of 6.5  $\text{\AA}$  for thick (125  $\text{\AA}$ ) films.<sup>21</sup> Our results for the width are reported in Table II as a function of the number of particles in the slab  $N$ ; the size of each slab is given in terms of  $z_{1/2}$ , defined as the value of  $z$  in which the density is half the density in the inner part  $\rho_0$ . The results contained in the Table have been extracted from the DMC density profile by performing a fit with the asymmetric form given by Eq. (18). If the fit is symmetric ( $\delta = 1$ ),  $W$  is reduced with respect to the values reported in the Table but the differences are only  $\sim 0.1$   $\text{\AA}$  since the degree of asymmetry is rather small.

The main prediction of the present study would be the value of  $W$  corresponding to a free surface, with a central density equal to the bulk equilibrium value  $\rho_0^{\text{bulk}} = 0.02186$   $\text{\AA}^{-3}$ . However, the values reported in Table II show a dependence on the size of the slab, even for the largest ones, which makes difficult that estimation. In order to shed light on this dependence, and trying to analyze possible extrapolations to larger slabs, the

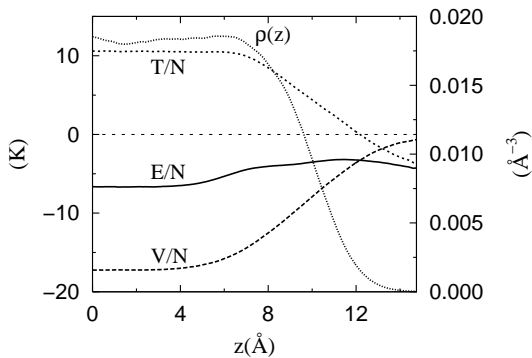


FIG. 5:  $z$ -dependence of the total ( $E/N$ ), kinetic ( $T/N$ ), and potential ( $V/N$ ) energies in the slab geometry. The behavior of the energies is compared with the density profile (right scale). The data corresponds to a calculation with  $N = 108$  atoms.

results of the width  $W$  are shown as a function of  $z_{1/2}$  in Fig. 4. After testing different analytical forms, we have arrived to a rather simple model that describes quite accurately the DMC data,

$$W(z) = W_\infty \left(1 - e^{-b\sqrt{z}}\right), \quad (19)$$

$W_\infty$  being the predicted width of the free surface. The value obtained is  $W_\infty = 6.3(4)$  Å. In Fig. 4, experimental results from Penanen *et al.*,<sup>21</sup> corresponding to thick  $^4\text{He}$  films adsorbed on a solid substrate at  $T = 0.45$  K, are also shown. If the DMC and experimental data are fitted altogether, according to the empirical law (19), the interfacial width of the free surface becomes  $W_\infty = 6.2(1)$  Å which is compatible with the extrapolated value considering only the theoretical results. Both extrapolations are in agreement with the width measured directly for the thickest film of 125 Å,  $W = 6.5 \pm 0.5$  Å.

The transition from a constant density in the central part of the slab to a zero density in the outer part of the surface implies a  $z$ -dependence in other magnitudes, in particular in the total and partial energies. In Fig. 5, this  $z$  dependence is shown in comparison with  $\rho(z)$  for a  $N = 108$  slab. The three functions  $E/N(z)$ ,  $V/N(z)$ , and  $T/N(z)$  are calculated by averaging the energies of particles located between  $z$  and  $z + \Delta z$  according to a uniform grid with  $\Delta z \simeq 0.1$  Å and, therefore, they are not exact estimations. Nevertheless, the residual bias coming from the trial wave function is expected to be small and the qualitative behavior would not change from the one reported in Fig. 5. As one can see, the potential energy evolves from a constant value in the inner part (corresponding to the bulk value at the central density of this slab) to zero when  $\rho(z) \rightarrow 0$ . Also the total and kinetic energies in the central part of the slab correspond to the bulk values but, approaching the surface, the total and kinetic energies reach the same constant value which

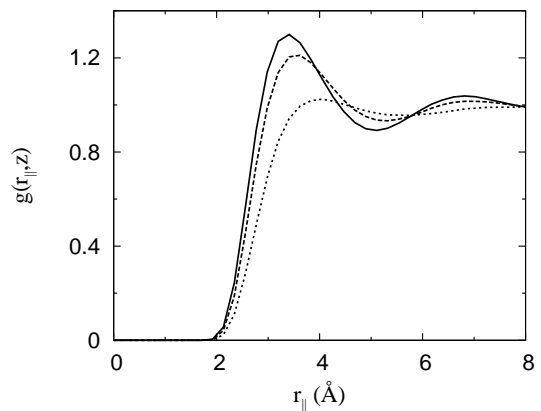


FIG. 6: Two-body radial distribution function for different values of  $z$ ,  $g(r_{||}, z)$ . Going from bottom to top in the height of the main peak the data corresponds to  $z = 11, 9.5,$  and  $2$  Å for a slab with 324 atoms.

is proportional to the analytic expression<sup>49,50</sup>

$$E/N(z) = T/N(z) \simeq \lim_{z \rightarrow \infty} -\frac{\hbar^2}{2m} \frac{\nabla^2 \sqrt{\rho(z)}}{\sqrt{\rho(z)}}. \quad (20)$$

### C. Distribution and structure functions

The slab geometry provides the opportunity of studying the density dependence of the spatial structure in a quantum liquid from bulk to zero densities. The  $z$ -dependence of the structure functions is analyzed by performing slices of variable width  $\Delta z$  (larger in the center of the slab and smaller in the surface) in which the density can be considered like a constant. The structure of the fluid is then calculated as a function of  $z$ , accumulating data corresponding to atoms localized between  $z$  and  $z + \Delta z$ . Following this scheme, we have calculated the two-body radial distribution function  $g(r_{||}, z)$  and the results obtained, for a selected set of  $z$  values, are reported in Fig. 6. The functions  $g(r_{||}, z)$  follow the evolution of the density: by increasing  $z$  (decreasing  $\rho$ ) the height of the main peak decreases and moves to larger  $r_{||}$  values, reaching in the outer part of the surface a very low density regime where  $g(r_{||}, z)$  resembles the typical result for a dilute gas.

Additional information on the structure of the system, and on its excitation modes, are contained in the  $z$ -dependent static structure factor. In its general form it is defined as

$$S(k_{||}, z, z') = \frac{1}{[N(z) N(z')]^{1/2}} \langle \rho_{\mathbf{k}_{||}}(z) \rho_{-\mathbf{k}_{||}}(z') \rangle, \quad (21)$$

$\rho_{\mathbf{k}_{||}}(z) = \sum_{i=1}^{N(z)} e^{i\mathbf{k}_{||} \cdot \mathbf{r}_i}$  being the fluctuation density operator for all the particles  $N(z)$  in the slice  $(z, z + \Delta z)$ , and  $\mathbf{k}_{||}$  a momentum in the  $x-y$  plane. Our calculations have addressed only the diagonal part of this function,  $z = z'$ , which in a simplified notation are called  $S(k_{||}, z)$

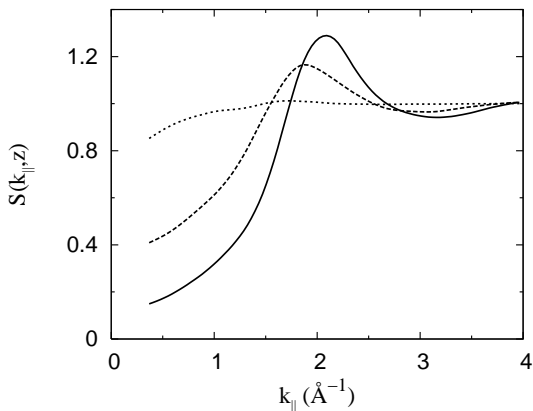


FIG. 7: Static structure function for different values of  $z$ ,  $S(k_{\parallel}, z)$ . Going from bottom to top in the height of the main peak the data corresponds to  $z = 11, 9.5, \text{ and } 2 \text{ \AA}$  for a slab with 324 atoms.

in this work. Results for  $S(k_{\parallel}, z)$ , corresponding to the same slices chosen for  $g(r_{\parallel}, z)$  in Fig. 6, are shown in Fig. 7. The evolution of  $S(k_{\parallel}, z)$  with  $z$  follows the same trends observed in Fig. 6 for  $g(r_{\parallel}, z)$ , i.e., a behavior essentially determined by the local density in each slice  $\rho(z)$ . The behavior when  $k_{\parallel} \rightarrow 0$  is known to be different in the central part and in the surface of the slab. In the central part, where the mean density is constant, the static structure factor must show a linear behavior with  $k_{\parallel}$ , corresponding to the phonon mode of the homogeneous liquid. On the contrary, in the surface  $S(k_{\parallel}, z)$  diverges as  $1/\sqrt{k_{\parallel}}$  due to the presence of ripples.<sup>51</sup> The DMC results shown in Fig. 7 do not show signatures of ripples due probably to restrictions imposed on the lowest  $k_{\parallel}$  value accessible with a finite number of particles. Recent results for the structure function,<sup>33</sup> using path integral Monte Carlo (PIMC) with a number of particles larger than the one used in this work, show a change of behavior for the smallest  $k_{\parallel}$  values and for the most external slices that could be compatible with the singular behavior induced by ripples. Notwithstanding, the size of this signal observed in the PIMC results is appreciably reduced with respect to a VMC calculation, using shadow wave functions, which emphasized the importance of ripples for a correct description of the  $^4\text{He}$  surface.<sup>36</sup>

#### D. Condensate fraction

The presence of off-diagonal long-range order (ODLRO) in a Bose liquid is one of its more essential properties.<sup>14</sup> The measure of ODLRO in the system is quantified by the Bose-Einstein condensate fraction  $n_0$ , i.e., the fraction of particles occupying the zero-momentum state. This information is contained in the one-body density matrix

$$\rho(\mathbf{r}_1, \mathbf{r}'_1) = \quad (22)$$

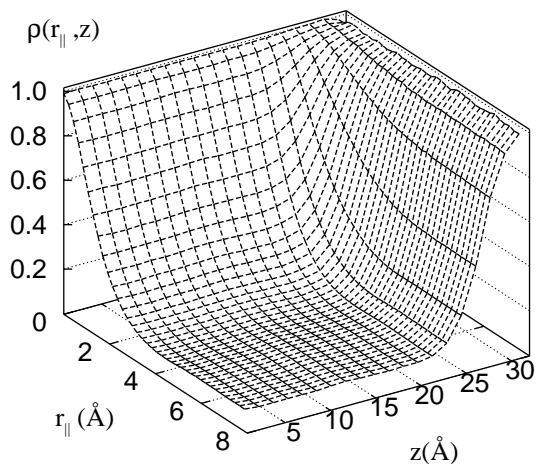


FIG. 8: One-body density matrix in a  $^4\text{He}$  slab with  $N = 324$ .

$$N \int d\mathbf{r}_2 \dots \mathbf{r}_N \Psi(\mathbf{r}_1, \mathbf{r}_2, \dots, \mathbf{r}_N) \Psi(\mathbf{r}'_1, \mathbf{r}_2, \dots, \mathbf{r}_N).$$

The geometry of the slab makes possible to express the one-body density matrix as a function of  $r_{\parallel}$ ,  $z$ , and  $z'$ ,  $\rho(r_{\parallel}, z, z')$ . Restricting the analysis to the particular case  $z = z'$ , the long range behavior of  $\rho(r_{\parallel}, z)$  gives the local condensate fraction  $n_0(z)$ ,

$$n_0(z) = \lim_{r_{\parallel} \rightarrow \infty} \frac{\rho(r_{\parallel}, z)}{\rho(0, z)}. \quad (23)$$

The function  $\rho(r_{\parallel}, z)$  is sampled in DMC following the standard procedure, i.e. through the expected value

$$\left\langle \frac{\psi(\mathbf{r}'_1, \mathbf{r}_2, \dots, \mathbf{r}_N)}{\psi(\mathbf{r}_1, \mathbf{r}_2, \dots, \mathbf{r}_N)} \right\rangle, \quad (24)$$

accumulating data for a set of slices in the  $z$  direction as explained in the previous subsection. Results for  $\rho(r_{\parallel}, z)$ , corresponding to the largest slab ( $N = 324$ ), are shown in Fig. 8. In this 3D picture, one can see the constant regime achieved for any  $z$  value when  $r_{\parallel} \rightarrow \infty$ , which corresponds to the condensate fraction  $n_0(z)$  (23). Following the evolution of  $n_0(z)$  with increasing  $z$ , one observes a large enhancement approaching the surface up to values close to 1 which would correspond to a fully Bose-condensed state.

The change in the condensate fraction as the surface is approached is more clearly shown in Fig. 9. In the inner part of the slab, where the mean density is very close to the bulk equilibrium density,  $n_0(z)$  is constant and equal to 0.095(5). When the density starts to decrease,  $n_0(z)$  increases up to almost 1. This result is not surprising since it is well known from bulk calculations that  $n_0$  decreases monotonically with the density. Possible density fluctuations in the surface, due to the presence of ripples (surface excited modes), that can suppress this nearly Bose-condensate state are not present in our calculations because the goal of the present work is the



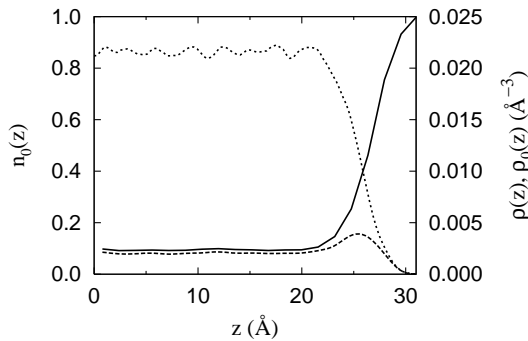


FIG. 9:  $z$  dependence of the condensate fraction in a  ${}^4\text{He}$  slab with  $N = 324$  (solid line, left scale). The condensate density  $\rho_0(z)$  (long-dashed line) and density profile  $\rho(z)$  (short-dashed line) are also shown (right scale).

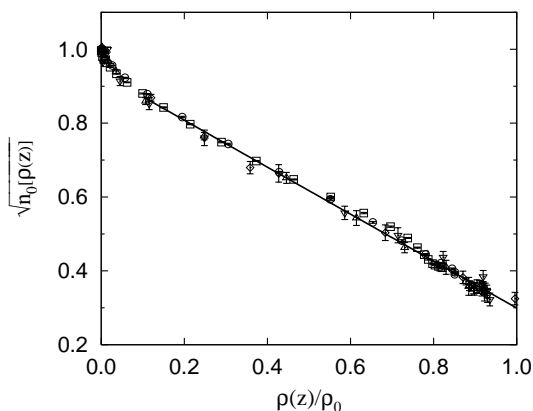


FIG. 10: Condensate amplitude  $\sqrt{n_0[\rho(z)]}$  as a function of the density  $\rho(z)/\rho_0$ , with  $\rho_0$  the bulk equilibrium density. The points correspond to estimations of the condensate fraction for all the slabs studied. The solid line corresponds to the analytical fit (25) to data in the density range  $0.1 \leq \rho(z)/\rho_0 \leq 1$ .

ground state of the free  ${}^4\text{He}$  surface. At low temperatures, the influence of ripplons in  $n_0(z)$  has been studied by Draeger and Ceperley using the PIMC method;<sup>33</sup> their results show an at most 20 % reduction of  $n_0$ , with effects only at extremely low density where, on the other hand, the statistical signal is rather poor. Figure 9 also contains the evolution with  $z$  of the condensate density,  $\rho_0(z) = n_0(z)\rho(z)$ , which shows a clear maximum at approximately  $z_{1/2}$  and then becomes equal to the total density when  $\rho(z) \rightarrow 0$ . The resulting picture is in an overall agreement with the VMC results of Lewart and Pandharipande<sup>37</sup> and with recent DMC studies of trapped hard-core bosons by DuBois and Glyde.<sup>52</sup>

Collecting data for  $n_0$  as a function of the density, and for the different slabs calculated, one can try to elucidate if they can be well reproduced by a single analytical form. This was already analyzed by Lewart *et al.*<sup>37</sup> in a VMC calculation of natural orbitals in  ${}^4\text{He}$  clusters. They observed that the condensate fraction for all the clusters

studied could be rather well described by the law

$$\sqrt{n_0[\rho(z)]} = A - B \frac{\rho(z)}{\rho_0}. \quad (25)$$

The function  $\sqrt{n_0[\rho(z)]}$  can be seen as a condensate amplitude assuming that  $\rho_0(z) \simeq |\Psi_0(z)|^2$ , with  $\Psi_0(z)$  the condensate wave function. The present results for  $\sqrt{n_0[\rho(z)]}$ , including the data for all the slabs, are reported in Fig. 10 as a function of  $\rho(z)/\rho_0$ ,  $\rho_0$  being the equilibrium density of bulk  ${}^4\text{He}$ . In the range  $0.1 \leq \rho(z)/\rho_0 \leq 1$  all the data shows the same linear behavior that can be very well fitted by the empirical law (25) with values  $A = 0.935$  and  $B = 0.636$ . As can be seen in Fig. 10, the DMC data departs from this linear behavior at very low densities  $\rho(z)/\rho_0 < 0.1$ , approaching faster to the zero value at zero density.

#### IV. DISCUSSION

Using a slab geometry we have presented in this work a DMC study of the ground-state properties of the free  ${}^4\text{He}$  surface. The interatomic potential is highly accurate, and in the past has allowed for an excellent reproduction of the experimental equation of state in the bulk phase.<sup>41</sup> We believe that the combination of an essentially exact method and this very well know interaction between helium atoms guarantees the accuracy of a microscopic description of the kind intended here. At this point it is interesting to compare the main results obtained with available experimental data.

The value of the surface tension of superfluid  ${}^4\text{He}$  at zero temperature is one of the main results. Our prediction,  $\sigma = 0.281(3) \text{ K}\text{\AA}^{-2}$ , must be compared with the two available and different experimental measures,  $\sigma = 0.257 \pm 0.001 \text{ K}\text{\AA}^{-2}$  and  $\sigma = 0.274 \pm 0.002 \text{ K}\text{\AA}^{-2}$ .<sup>24,25</sup> Both experimental determinations correspond to zero temperature extrapolations using measured values for  $\sigma(T)$  and the Atkins ripplon law for  $\sigma(T)$  at very low temperatures.<sup>13</sup> Our theoretical result is larger than both measures but it is nearly statistically compatible with the value  $\sigma = 0.274 \text{ K}\text{\AA}^{-2}$  obtained by Roche *et al.*<sup>25</sup> It is worth noticing that most of theoretical estimations of  $\sigma$  agree with this larger experimental value.

A second result which can be compared with experiment is the surface width  $W$ . Obviously, the most relevant result would be the *real* width of the surface, i.e., the asymptotic width for thick slabs. In our results,  $W$  shows a dependence with the size of the slab and, even for the largest one, this asymptotic regime is not achieved. For the  $N = 324$  slab the width is  $5.07(5) \text{ \AA}$ . Using a reasonable fit to the data we can estimate the asymptotic surface width, the value obtained being  $W_\infty = 6.3(4) \text{ \AA}$  which is in good agreement with a recent experimental measure at  $T = 0.44 \text{ K}$  for a  $125 \text{ \AA}$  film,  $W = 6.5 \pm 0.5 \text{ \AA}$ .<sup>21</sup> On the other hand, the density profiles, specially the ones with a greater number of particles, show a slight asymmetry with a deeper slope in the outer

part of the surface. This possible asymmetry, observed also in other theoretical approaches,<sup>16,30</sup> was analyzed in an x-ray specular reflectivity experiment by Lurio *et al.*<sup>20</sup> but uncertainties in the scattering amplitude made impossible a clean answer to this point.

Last but not least there is the question of the enhancement of the condensate fraction in the surface. The experimental measure of  $n_0$  in liquid  $^4\text{He}$  has been elusive for long time due to its small value.<sup>53</sup> Nowadays, deep inelastic neutron scattering has largely improved both its efficiency and data analysis and therefore there is much more confidence on the results obtained. Recently, Pearce *et al.*<sup>40</sup> have carried out neutron scattering experiments on liquid  $^4\text{He}$  adsorbed in thick layers on an MgO substrate. The analysis of the dynamic structure function obtained for different number of layers shows unambiguously an increase of the Bose condensate when the

number of layers is reduced. The data obtained are somehow not completely accurate at the quantitative level but the main conclusion of the experiment, i.e., the enhancement of  $n_0$  in the surface, is in agreement with our (and others<sup>33,37</sup>) theoretical calculations. It is worth mentioning that signatures of a large condensate fraction have been also observed by Wyatt<sup>39</sup> in quantum evaporation experiments.

### Acknowledgments

We acknowledge financial support from DGI (Spain) Grant No. BFM2002-00466 and Generalitat de Catalunya Grant No. 2001SGR-00222.

- 
- <sup>1</sup> *Microscopic Approaches to Quantum Liquids in Confined Geometries*, ed. by E. Krotscheck and J. Navarro (World Scientific, Singapore, 2002).
- <sup>2</sup> B. E. Clements, J. L. Epstein, E. Krotscheck, and M. Saarela, *Phys. Rev. B* **48**, 7450 (1993).
- <sup>3</sup> B. E. Clements, E. Krotscheck, and M. Saarela, *Phys. Rev. B* **55**, 5959 (1997).
- <sup>4</sup> See special number of *J. Chem. Phys.* **115** (2001).
- <sup>5</sup> M. H. W. Chan, K. I. Blum, S. Q. Murphy, G. K. S. Wong, and J. D. Reppy, *Phys. Rev. Lett.* **61**, 1950 (1988).
- <sup>6</sup> G. M. Zassenhaus and J. D. Reppy, *Phys. Rev. Lett.* **83**, 4800 (1999).
- <sup>7</sup> H. R. Glyde, O. Plantevin, B. Fåk, G. Coddens, P.S. Danielson, and H. Schober, *Phys. Rev. Lett.* **84**, 2646 (2000).
- <sup>8</sup> W. Teizer, R. B. Hallock, E. Dujardin, and T. W. Ebbesen, *Phys. Rev. Lett.* **82**, 5305 (1999); *Phys. Rev. Lett.* **84**, 1844 (2000).
- <sup>9</sup> J. C. Lasjaunias, K. Biljaković, J. L. Sauvajol, and P. Monceau, *Phys. Rev. Lett.* **91**, 025901 (2003).
- <sup>10</sup> G. Stan and M. W. Cole, *Surf. Sci.* **395**, 280 (1998).
- <sup>11</sup> M. C. Gordillo, J. Boronat, and J. Casulleras, *Phys. Rev. B* **61**, R878 (2000).
- <sup>12</sup> M. Aichinger, S. Kilić, E. Krotscheck, and L. Vranješ, *Phys. Rev. B* **70**, 155412 (2004).
- <sup>13</sup> D. O. Edwards and W. F. Saam, in *Progress in Low Temperature Physics*, ed. by D. F. Brewer (North-Holland, Amsterdam, 1978), Vol. 7A.
- <sup>14</sup> C. E. Campbell, in *Recent Progress in Many-Body Theories*, ed. by E. Schachinger *et al.* (Plenum Press, New York, 1995), Vol. 4.
- <sup>15</sup> K. A. Gernoth, J. W. Clark, G. Senger, and M. L. Ristig, *Phys. Rev. B* **49**, 15836 (1994).
- <sup>16</sup> F. Dalfovo, A. Lastrì, L. Pricapenko, S. Stringari, and J. Treiner, *Phys. Rev. B* **52**, 1193 (1995).
- <sup>17</sup> J. Harms, J. Peter Toennies, and F. Dalfovo, *Phys. Rev. B* **58**, 3341 (1998).
- <sup>18</sup> J. Harms, J. Peter Toennies, M. Barranco, and M. Pi, *Phys. Rev. B* **63**, 184513 (2001).
- <sup>19</sup> L. B. Lurio, T. A. Rabedeau, P. S. Pershan, I. F. Silvera, M. Deutsch, S. D. Kosowsky, and B. M. Ocko, *Phys. Rev. Lett.* **68**, 2628 (1992).
- <sup>20</sup> L. B. Lurio, T. A. Rabedeau, P. S. Pershan, I. F. Silvera, M. Deutsch, S. D. Kosowsky, and B. M. Ocko, *Phys. Rev. B* **48**, 9644 (1993).
- <sup>21</sup> K. Penanen, M. Fukuto, R. K. Heilmann, I. F. Silvera, and P. S. Pershan, *Phys. Rev. B* **62**, 9621 (2000).
- <sup>22</sup> D. V. Osborne, *J. Phys.: Condens. Matter* **1**, 289 (1989).
- <sup>23</sup> A. T. van Urk, W. H. Keesom, and H. K. Onnes, *Proc. R. Acad. Sci. Amsterdam* **28**, 58 (1925).
- <sup>24</sup> M. Iino, M. Suzuki, and A. J. Ikushima, *J. Low Temp. Phys.* **63**, 495 (1985).
- <sup>25</sup> P. Roche, G. Deville, N. J. Appleyard, and F. I. B. Williams, *J. Low Temp. Phys.* **106**, 565 (1997).
- <sup>26</sup> K. Nakanishi and M. Suzuki, *J. Low Temp. Phys.* **113**, 585 (1998).
- <sup>27</sup> C. Vicente, W. Yao, H. J. Maris, and G. M. Seidel, *Phys. Rev. B* **66**, 214504 (2002).
- <sup>28</sup> A. Guirao, M. Centelles, M. Barranco, M. Pi, A. Polls, and X. Viñas, *J. Phys.: Condens. Matter* **4**, 667 (1992).
- <sup>29</sup> L. Szybisz, *Eur. J. Phys. B* **14**, 733 (2000).
- <sup>30</sup> S. A. Chin and E. Krotscheck, *Phys. Rev. B* **45**, 852 (1992).
- <sup>31</sup> S. C. Pieper, R. B. Wiringa, and V. R. Pandharipande, *Phys. Rev. B* **32**, 3341 (1985).
- <sup>32</sup> J. L. Vallés and K. E. Schmidt, *Phys. Rev. B* **38**, 2879 (1988).
- <sup>33</sup> E. W. Draeger and D. M. Ceperley, *Phys. Rev. Lett.* **89**, 015301 (2002).
- <sup>34</sup> E. Krotscheck, in *Microscopic Approaches to Quantum Liquids in Confined Geometries*, ed. by E. Krotscheck and J. Navarro (World Scientific, Singapore, 2002).
- <sup>35</sup> *Monte Carlo Methods in Ab Initio Quantum Chemistry*, B. L. Hammond, W. A. Lester Jr., and P. J. Reynolds (World Scientific, Singapore, 1994).
- <sup>36</sup> D. E. Galli and L. Reatto, *J. Phys.: Condens. Matter* **12**, 6009 (2000).
- <sup>37</sup> D. S. Lewart, V. R. Pandharipande, and S. C. Pieper, *Phys. Rev. B* **37**, 4950 (1988).
- <sup>38</sup> A. Griffin and S. Stringari, *Phys. Rev. Lett.* **76**, 259 (1996).
- <sup>39</sup> A. F. G. Wyatt, *Nature* **391**, 6662 (1998).
- <sup>40</sup> J. V. Pearce, S. O. Diallo, H. R. Glyde, R. T. Azuah, T. Arnold, and J. Z. Larese, *J. Phys.: Condens. Matter* **16**,

- 4391 (2004).
- <sup>41</sup> J. Boronat, in *Microscopic Approaches to Quantum Liquids in Confined Geometries*, ed. by E. Krotscheck and J. Navarro (World Scientific, Singapore, 2002).
- <sup>42</sup> J. Boronat and J. Casulleras, Phys. Rev. B **49**, 8920 (1994).
- <sup>43</sup> L. Reatto, Nucl. Phys. **A328**, 253 (1979).
- <sup>44</sup> K. S. Liu, M. H. Kalos, and G. V. Chester, Phys. Rev. B **12**, 1715 (1975).
- <sup>45</sup> R. A. Aziz, F. R. W. McCourt, and C. C. K. Wong, Mol. Phys. **61**, 1487 (1987).
- <sup>46</sup> R. A. Aziz, V. P. S. Nain, J. S. Carley, W. L. Taylor, and G. T. McConville, J. Chem. Phys. **70**, 4330 (1979).
- <sup>47</sup> J. Casulleras and J. Boronat, Phys. Rev. B **52**, 3654 (1995).
- <sup>48</sup> T. Regge, J. Low Temp. Phys. **9**, 123 (1972).
- <sup>49</sup> I. B. Mantz and D. O. Edwards, Phys. Rev. B **20**, 4518 (1979).
- <sup>50</sup> A. Belić, F. Dalfovo, S. Fantoni, and S. Stringari, Phys. Rev. B **49**, 15253 (1994).
- <sup>51</sup> E. Krotscheck, S. Stringari, and J. Treiner, Phys. Rev. B **35**, 4754 (1987).
- <sup>52</sup> J. L. DuBois and H. R. Glyde, Phys. Rev. A **63**, 023602 (2001).
- <sup>53</sup> *Excitations in Liquid and Solid Helium*, H. R. Glyde (Clarendon Press, Oxford, 1994).